Analyst

ROYAL SOCIETY OF CHEMISTRY

CRITICAL REVIEW

View Article Online
View Journal | View Issue

Cite this: *Analyst*, 2024, **149**, 1381

Design and application of dual-emission metal–organic framework-based ratiometric fluorescence sensors

Shuxin Zhang, Jingyu Xiao, Geng Zhong, Tailin Xu * and Xueji Zhang*

Metal–organic frameworks (MOFs) are novel inorganic–organic hybridized crystals with a wide range of applications. In the last twenty years, fluorescence sensing based on MOFs has attracted much attention. MOFs can exhibit luminescence from metal nodes, ligands or introduced guests, which provides an excellent fluorescence response in sensing. However, single-signal emitting MOFs are susceptible to interference from concentration, environment, and excitation intensity, resulting in poor accuracy. To overcome the shortcomings, dual-emission MOF-based ratiometric fluorescence sensors have been proposed and rapidly developed. In this review, we first introduce the luminescence mechanisms, synthetic methods, and detection mechanisms of dual-emission MOFs, highlight the strategies for constructing ratiometric fluorescence sensors based on dual-emission MOFs, and classify them into three categories: intrinsic dual-emission and single-emission MOFs with luminescent guests, and non-emission MOFs with other luminescent materials. Then, we summarize the recent advances in dual-emission MOF-based ratiometric fluorescence sensors in various analytical industries. Finally, we discuss the current challenges and prospects for the future development of these sensors.

Received 19th December 2023,
Accepted 21st January 2024

DOI: 10.1039/d3an02187d

rsc.li/analyst

1. Introduction

Metal–organic frameworks (MOFs) are a new class of porous materials formed by self-assembly through coordination bonds between metal nodes/clusters and organic linkers.[1] In general, transition metal ions with unfilled d orbitals are selected as metal centers to accept lone pairs of electrons from ligands, and ligands containing at least one polydentate functional group are selected to decoordinate metal ions.[2] Due to advantages such as simple synthesis routes, large specific surface areas, high porosities, and easy modifications, MOFs have been widely used in the fields of gas storage and separation,[3–5] catalysis,[6–8] sensing,[9–11] and drug delivery.[12–14] In these applications, the use of MOFs as fluorescent materials to construct sensors for a variety of targets is popular due to

School of Biomedical Engineering, Health Science Center, Shenzhen University, Shenzhen 518060, China. E-mail: xutailin@szu.edu.cn, zhangxueji@szu.edu.cn

Shuxin Zhang

Shuxin Zhang is currently pursuing his PhD at Shenzhen University. He received his M.S. degree in Bioresource Chemistry from Sichuan Agricultural University. His research interests include the construction of ultrasensitive fluorescence biosensors and bioanalytical chemistry.

Jingyu Xiao

Jinyu Xiao is currently a postdoctoral fellow at Shenzhen University. She received her PhD in Chemistry from the University of Science and Technology Beijing. Her research interests include smart wearable biosensors and bioelectroanalytical chemistry.

the following advantages: (i) MOF-based fluorescence sensors are faster and easier to analyze than conventional methods such as high-performance liquid chromatography (HPLC) and gas chromatography/mass spectrometry (GC/MS);[15] (ii) the large specific surface area and high porosity of MOF materials can enrich analytes and fully interact with each other, thus increasing the sensitivity of the sensors;[16] (iii) MOFs with tunable pore sizes and structural diversity facilitate the matching of a wider range of guests, thus expanding the range of sensing applications;[17] (iv) their luminescence, chemical and physical properties can be altered by changing metal ions, organic ligands, or guests to achieve specific response to target species.[18,19]

However, MOF-based single-emission fluorescence sensors are susceptible to be affected by a variety of factors such as sensor concentration, background fluorescence and instrument parameters, leading to erroneous detection results. To avoid this circumstance, there is an increasing focus on dual-emission MOF-based ratiometric fluorescence sensors. Since sensors are used to measure analytes with the ratio of signal intensities at two different wavelengths and signal fluctuations caused by non-analytical factors are minimized by a self-correction function, rationally designed MOF-based ratiometric fluorescence sensors have highly accurate detection performance. In addition, the sensors with strong visible colour changes are more sensitive and useful for on-site visualisation.[20] Hence, dual-emission MOF-based ratiometric fluorescence sensing has achieved rapid development in recent years.

In this review, as shown in Fig. 1, we emphasized the design strategies of dual-emission MOFs and their sensing applications for various targets such as pH, temperature, ions, biomarkers, *etc.*, over the last 5 years. In addition, we discuss the challenges that the sensors still face today and the prospects in future research areas.

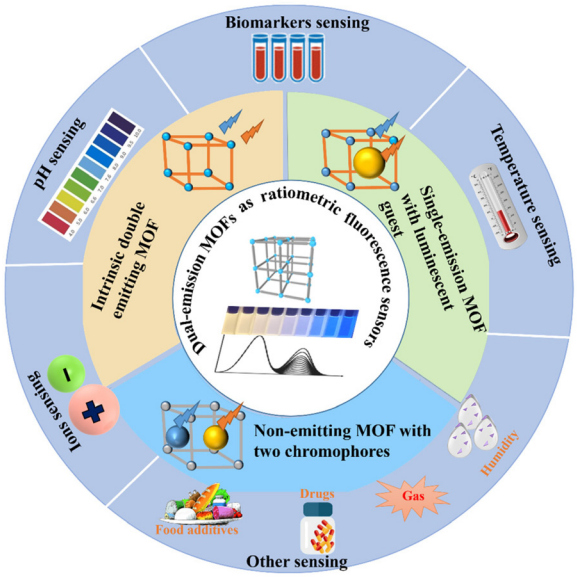

Fig. 1 Schematic diagram of the construction strategy and the latest application of the dual-emission MOF-based ratiometric sensors.

2. Luminescence mechanism of dual-emission MOFs

MOFs can be assembled using suitable metal ions and various functional ligands. The covalent bonding between the ligand and the metal allows the metal ion, ligand or guest molecule to confer different fluorescence properties to MOFs. Additionally, metal-to-ligand charge transfer between ligands and metals also produces fluorescence. Therefore, MOFs provide an ideal platform for the development of solid-state luminescent materials. As shown in Fig. 2, the emission mechanisms of tunable dual-emission MOFs primarily encom-

Geng Zhong

Geng Zhong is currently pursuing his master's degree at Shenzhen University. He received his B.S. degree in Computer Science and Technology from Guangdong University of Finance and Economics. His research interests are wearable biosensors and electrochemical detection.

Tailin Xu

Tailin Xu is an Associate Professor at the School of Biomedical Engineering, Health Science Center, Shenzhen University. He joined the Research Center for Bioengineering & Sensing Technology research group at the University of Science & Technology Beijing to pursue his Ph.D. degree, where he studied until 2017. In 2013, he joined Joseph Wang's group as a joint Ph.D. student at the University of California, San Diego, where he studied until 2015. His research interests include wearable sensors, biointerfaces, and functional nanomotors.

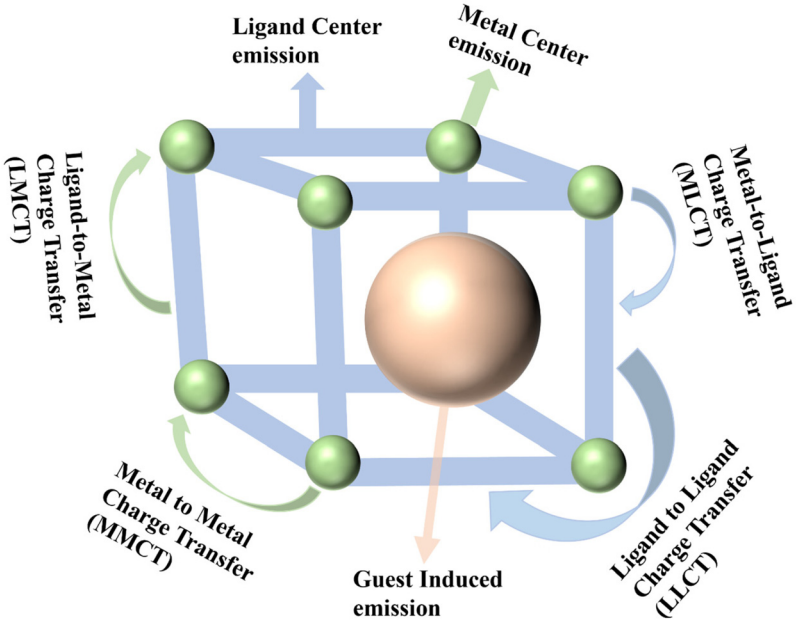

Fig. 2 Schematic representation of the various origins of photoluminescence in a porous MOF. Green ball: metal node; blue cylinder: organic connector; yellow ball: guest in MOFs.

pass three types: metal-centered (MC) emission, ligand-centered (LC) emission, and guest-induced emission.

2.1 Metal centered emission

MC emission is commonly observed in lanthanide metal–organic frameworks (Ln-MOFs). In Ln-MOFs, due to the Laporte-forbidden f–f transitions, direct excitation of lanthanide ions is hindered, leading to low absorption efficiency. Therefore, the luminescence of lanthanide ions requires sensitization by organic ligands. Ligands with free carboxyl groups can coordinate with lanthanide ions. These ligands can either promote or disrupt energy transfer processes, facilitating the transfer of energy from the ligand to the lanthanide ions, thereby enhancing their light absorption capabilities. Above phenomenon is widely known as the "antenna effect".[21]

2.2 Ligand centered emission

Organic ligands play a crucial role in the photoluminescence behaviour of luminescent MOFs. In particular, π-electron-rich ligands are capable of absorbing UV-visible light and achieving radiative transitions *via* fluorescence or phosphorescence. When there is no significant charge transfer (CT) or resonance energy transfer (RET) between the ligand and the metal center, the luminescence properties of MOFs are consistent with those of the original ligand. When CT occurs between the metal and the ligand, *i.e.*, metal-to-ligand charge transfer (MLCT) and ligand-to-metal charge transfer (LMCT), the energy level of the ligand is slightly disturbed resulting in a slight shift of the emission wavelength. In addition, CT or RET, *i.e.*, ligand-to-ligand charge transfer (LLCT) or ligand-to-ligand resonance energy transfer (LLRET), can exist between different ligands, and the fluorescence intensity and wavelength of the ligand are altered.[22]

2.3 Guest or adsorbed luminophore-based emission

MOFs can combine with a wide range of guest molecules to create diverse composites. Luminescent composites are achieved by embedding or adsorbing chromophores, such as dyes, quantum dots, or luminescent nanomaterials, inside or on the surface of MOFs. The luminescence properties of these composites can be independent or interact with each other. In

Xueji Zhang

Xueji Zhang is the Vice President of Shenzhen University and the national chair professor & director of Research Center for Bioengineering and Sensing Technology, University of Science & Technology Beijing. He obtained his Ph.D. from Wuhan University in 1994. He was a postdoc fellow at the National Institute of Chemistry, Slovenia, Swiss Federal Institute of Technology (ETH), Zurich, and New Mexico State University from 1995–1999. He has worked at World Precision Instruments Inc. as a Sr. Scientist, the head of chemistry department, and Sr. Vice President of science, respectively, since 1998. His research has been centered on electrochemistry, bioanalysis, micro/nanosensors, and biomedical instrumentation.

the independent case, MOFs and the encapsulated guest maintain their original luminescence properties, while in the case of mutual influence, luminescence is achieved mainly through the fluorescence resonance energy transfer (FRET) mechanism. In this process, if the emission spectrum of the energy donor overlaps with the absorption spectrum of the energy acceptor and the distance between the two is less than 10 nm, FRET can be triggered, resulting in the weakening of the fluorescence intensity of the donor and the simultaneous excitation of the luminescence of the acceptor. Notably, the FRET efficiency between MOFs and the guest can be precisely modulated by adjusting the type or concentration of the guest.[23]

3. Synthesis methods of dual-emission MOFs

The typical strategies for preparing dual-emission MOFs include: (1) one-pot method: most luminescent MOFs are prepared by a simple one-pot liquid-phase thermal self-assembly of soluble precursors containing organic ligands and metal ions. This strategy can also be used to construct dual-emission MOFs with mixed metals or ligands, and MOFs encapsulating luminescent guests;[24,25] (2) i*n situ* growth: benefiting from the uniform porosity of MOFs, small-sized luminescent guest materials can be effectively synthesized within the pores by the *in situ* reaction of introduced small molecule precursors, and the size of the guests can be precisely controlled by the size of the pores;[26] (3) ion exchange: luminescent MOFs with charged frameworks have strong electrostatic interactions with guests, allowing the encapsulation of ionic luminophores to form dual-emission center MOFs;[27] (4) post-synthetic modification: first, MOFs with a single luminescence property are synthesized, and then a second type of luminescent center is introduced or the existing luminescent center is adjusted by chemical modification.[20] These methods allow researchers to finely customize the structure of dual-emission MOFs, thereby facilitating in-depth studies of the luminescence mechanisms of MOFs.

4. Detecting mechanism of dual-emission MOF sensors

From the experimental results so far, the dual-emission MOF-based ratiometric fluorescence sensor modes can be grouped into three categories: (1) two emissions "turn off" and "turn on", one emission decreases while another increases; (2) two emissions with either "turn on" or "turn off", one emission changes (either increases or decreases) and while another remains constant; (3) two emissions undergo the same change, either increasing or decreasing, but to varying degrees. Specific receptor–target interactions can induce changes in the fluorescence signals of dual-emitting MOFs through different mechanisms. Here, we briefly describe four common detection mechanisms involved in most studies, including photoelectron transfer (PET), Förster resonance energy transfer (FRET), internal filtering effect (IFE), and target-induced chemical or structural changes in MOFs.

In PET, when a donor molecule is photoexcited, one of its excited electrons can jump from the donor's lowest unoccupied molecular orbital (LUMO) to the LUMO of the acceptor, leading to fluorescence quenching.[28,29] FRET is a common fluorescence sensing mechanism that works through a distance-dependent non-radiative energy transfer process. When the emission spectrum of the donor partially overlaps with the absorption spectrum of the acceptor, energy transfers from the donor to the acceptor through FRET.[30] The efficiency of FRET depends on several factors, including the extent of spectral overlap, the distance between the donor and acceptor, and their dipole–dipole interactions. Therefore, when the excitation spectrum of a target overlaps with the emission spectrum of MOFs, the presence of the target changes the fluorescence of the MOFs. IFE is a phenomenon that results in significant fluorescence quenching through the competitive absorption of excitation light between the analyte and MOFs or by absorbing the MOFs' fluorescence emission. In this case, the absorption spectrum of the analyte usually overlaps with the emission or absorption spectrum of the MOFs. Unlike PET and FRET, IFE does not depend on the distance between the two substances. Additionally, appropriate functional groups on ligands can alter the fluorescence characteristics of MOFs. These groups can act as active sites for specific target recognition through coordination or covalent interactions, thus affecting the MOFs' fluorescence. During the detection process, a target can also disrupt the framework of MOF-based composites by interacting with the metal nodes or ligands, altering the fluorescence signal.[31,32]

5. Strategies for the construction of dual-emission MOF-based ratiometric fluorescence sensors

In order to rationally design dual-emission MOF-based ratiometric fluorescence sensors, the strategies developed in previous work were classified into three categories based on the emission centers (Fig. 3): (1) MOFs with intrinsic double emission (from different metal centers or different organic ligand centers, or both the metal and ligand centers); (2) single-emission MOFs combined with luminescent guests; (3) non-emissive MOFs hybridized with two chromophores.

5.1 Preparation of intrinsic double-emission MOFs

5.1.1 Bimetallic-based MOFs. The doping of single-emission lanthanide metal–organic frameworks (Ln-MOFs) with a lanthanide ion of different fluorescence properties is the simplest way to construct the dual-emission MOF-based ratiometric fluorescence sensors.[33–35] As common luminescent lanthanide ions, Eu^{3+} and Tb^{3+} strongly emit red and green light, respectively, which belong to the visible region and are

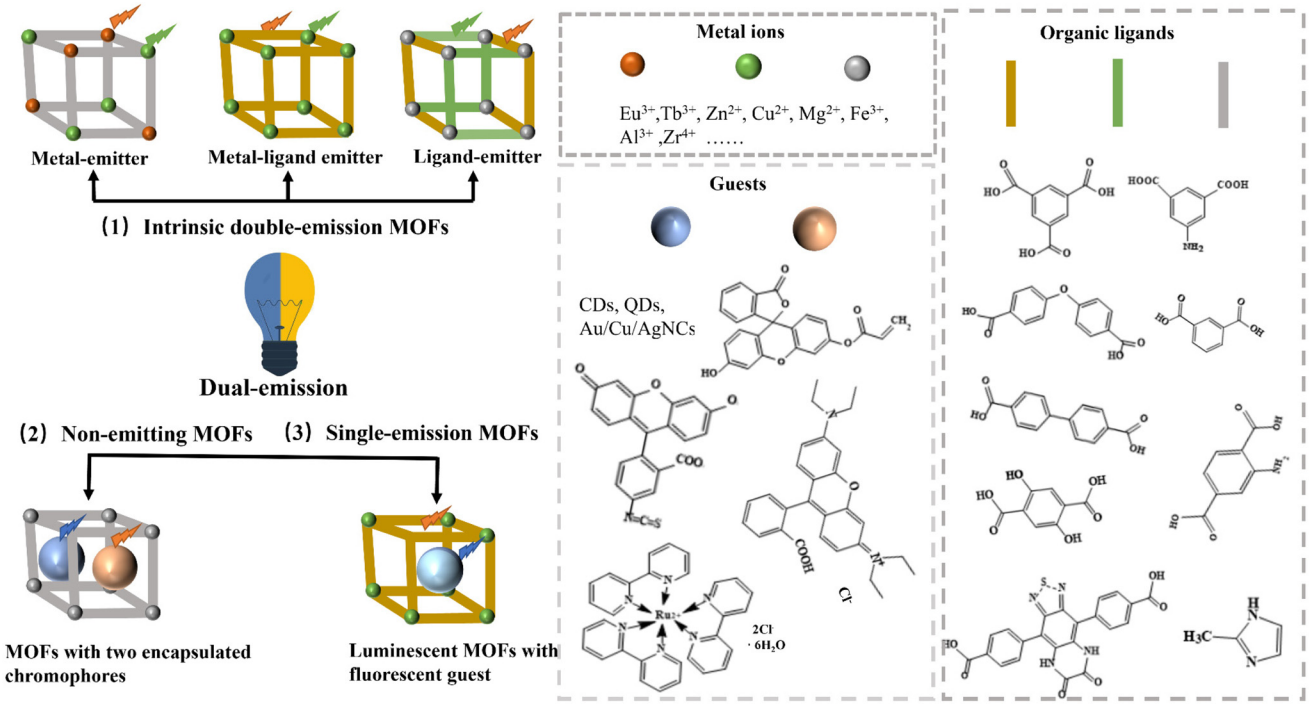

Fig. 3 Classification of design strategies for dual-emission MOF probes and common metal ions, organic ligands, and guests for the preparation of dual-emission MOFs.

widely used in the synthesis of luminescent materials.[36] The dual-emission intensity and the visible color of mixed Ln-MOFs can be adjusted by fine-tuning the ratio of emission centers Eu^{3+} to Tb^{3+}. As shown in Fig. 4A, a series of bimetallic Tb^{3+}/Eu^{3+} heterogeneous Ln-MOFs were prepared by grinding 1,3,5-benzenetricarboxylic acid (H_3BTC) and different ratios of Tb^{3+}/Eu^{3+} salts.[37] Due to the efficient antenna effect between H_3BTC and Tb^{3+}/Eu^{3+} as well as the energy transfer from Tb^{3+} to Eu^{3+}, the Eu/Tb-MOF exhibited strong green fluorescence of Eu^{3+} and weak red fluorescence of Tb^{3+}. The introduction of the target 2,6-dipicolinic acid (DPA) could better sensitize Tb^{3+} and inhibited the energy transfer from Tb^{3+} to Eu^{3+}, which strongly enhanced the fluorescence intensity of Tb^{3+}. As a result, the prepared bimetallic $Tb_{0.4}Eu_{0.6}$-MOF exhibited a sensitive ratiometric fluorescence sensing signal to DPA. A similar strategy has produced another series of bimetallic Ln-MOFs, called $\{(Me_2NH_2)\ [Tb_xEu_{(1-x)}(OBA)_2]\cdot(Hatz)\cdot(H_2O)_{1.5}\}_n$. As shown in Fig. 4B, the $Tb_{0.9}/Eu_{0.1}$-MOF with yellow fluorescence was chosen as a ratiometric fluorescence sensor with a pronounced response to methanol.[38] In addition, bimetallic Tb^{3+}/Eu^{3+} ions could also be introduced into the pores of non-emitting anionic MOFs by ion exchange to construct the ratiometric fluorescence sensor Tb/Eu@bio-MOF-1 that was sensitively responsive to DPA.[39]

5.1.2 Ligand-based MOFs. Organic ligands in MOFs are generally used as linkers to connect metal ions or metal clusters to form stable porous frameworks.[40] The integration of two fluorophore linkers with different luminescence properties into a single MOF structure makes it possible to construct ratiometric fluorescence sensors. For example, as shown in Fig. 4C, Wen *et al.* successfully prepared a dual-emission BDC/BDC-$(OH)_2$-MOF by a solvothermal method using 2-amino terephthalate (BDC-NH_2) and 2,5-dihydroxy terephthalate (BDC-$(OH)_2$) as fluorophore linkers and Zn^{2+} as the metal center.[41] Due to the selectivity of the $-NH_2$ groups on the surface of the BDC/BDC-$(OH)_2$-MOF, the dual-ligand emitting MOF was used as a ratiometric fluorescence sensor for HCHO and Fe^{3+} ions. In addition, a single ligand-based MOF can also exhibit two characteristic peaks of fluorescence. As an excited state intramolecular proton-transfer chromophore linker, 2,5-dihydroxyterephthalic acid (H_2DHT) has dual emission in proton solution with FQY < 1%.[42] Wang *et al.* prepared a fluorescent linker using benzothiadiazole (BTD) as the luminophore and tautomeric quinoxaline-2,3-(1*H*,4*H*)-dione (QD) as the reaction site, which was further integrated into a porous UiO-68 type zirconium metal–organic framework (MOF UiO-68-osdm). As a result, the MOF UiO-68-osdm could function as a ratiometric fluorescence sensor for visual and selective detection of alkyl amines.[43]

5.1.3 Metal and ligand-based MOFs. Insufficient energy transfer from an organic ligand to Ln^{3+} can generate MOFs with dual emission centers from both metal ions and ligands. A dual-emission Eu-MOF was prepared by using the 2-vinylterephthaliate (BDC-CH=CH_2) linker as the ligand, and due to the insufficient antenna effect between the ligand and Eu^{3+}, the Eu-MOF exhibited the fluorescence properties of both Eu^{3+} and BDC-CH=CH_2 (Fig. 4D). The addition of H_2S could enhance the blue fluorescence of the ligand BDC-CH=CH_2

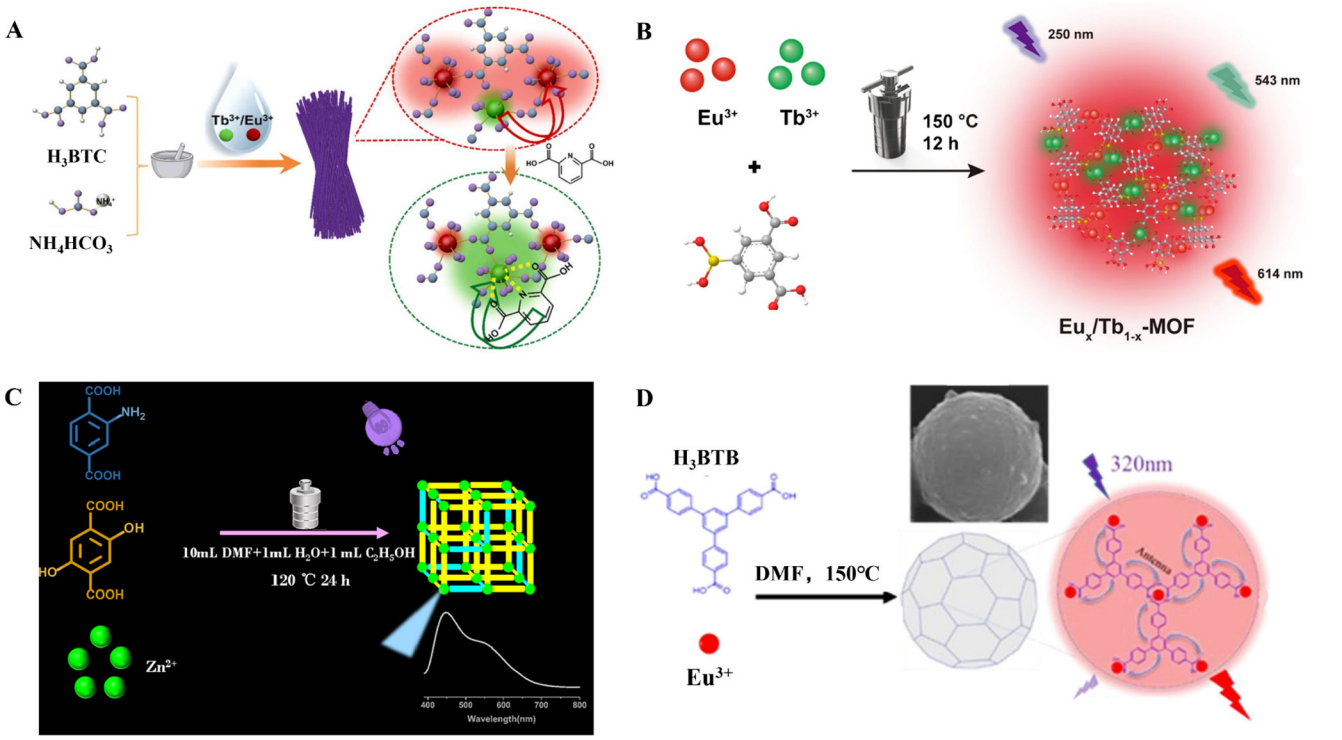

Fig. 4 Strategies for the construction of intrinsic dual-emission MOFs. Schematic preparation of bimetallic luminescent Tb_x/Eu_{1-x}-BTC (A) and (B) Eu_{1-x}/Tb_x-MOF.[37,38] (C) Schematic preparation of fluorophore linkers including BDC-NH_2 and BDC-$(OH)_2$ as blue and yellow emission assembly for dual-emission MOFs.[41] (D) Scheme illustration of luminescent Eu^{3+} and the emissive linker H_3BTB assembly for dual-emission MOFs.[44]

and reduce the red fluorescence of Eu^{3+} in the Eu-MOF, so the dual-emission Eu-MOF can be used as a ratiometric fluorescence sensor for H_2S detection.[44] Another Eu-MOF, $\{[Eu_2(L)_3\cdot(H_2O)_2\cdot(DMF)_2]\cdot 16H_2O\}_n$ (H_2L: 1,4-bis(5-carboxy-1*H*-benzimidazole-2-yl)benzene), also showed dual-emission fluorescence from both the organic ligand and Ln^{3+} centers.[45] In a word, all the above three strategies are able to construct dual-emission MOF-based ratiometric fluorescence sensors, but it is generally difficult to obtain intrinsic dual-emission MOFs with high quantum yields,[23] so the introduction of luminescent materials (dyes, nanoparticles and luminescent complexes) with high quantum yields into MOFs is very important in sensing applications.

5.2 Single-emissive MOFs with luminescent guests

As a novel porous material, MOFs provide a natural environment for guest molecules.[46] Dual-emission MOFs can be obtained by encapsulating luminescent guests (such as dyes, nanoparticles and complexes) into single-emission MOFs. The encapsulated luminescent guest is well dispersed in MOFs' ordered framework, which effectively prevents the aggregation-caused quenching (ACQ) of the luminescent guest in the free solid state.[47] In addition, the confinement effect of MOFs can reduce the molecular vibration of the luminescent guest, thus minimizing the non-radiative relaxation.[48]

5.2.1 Dyes@MOFs. Dyes are widely used as colorants, photosensitizers, and fluorescence sensors due to their high fluorescence quantum yield, but dyes have always faced the problem of aggregate quenching (ACQ).[49,50] Fortunately, MOFs have been explored for emitting fluorescence or phosphorescence light by integrating an emitting module into a framework, thus overcoming the ACQ effect of solid-state luminescent materials. As shown in Fig. 5A, Jiang *et al.* constructed a red-green dual-emission fluorescent composite RhB@MOFs with a FQY of around 25% by introducing a red organic fluorescent dye, rhodamine B (RhB), into metal–organic frameworks (Tb-MOFs). The complex was used as a ratiometric fluorescent probe for the detection of Fe^{3+} and AA with high sensitivity and good selectivity.[51] Zhou's group prepared NH_2-MOF by encapsulating the fluorescent dye eosin Y (EY) into an MIL-101 aluminum-based metal–organic framework (NH_2-MOF) with ligand luminescence, and NH_2-MOF could stably immobilize the EY molecules in the cavity and effectively inhibit the ACQ behavior of EY molecules. The obtained EY@MOF composites exhibited dual-emission fluorescence peaks at 437 nm and 565 nm, respectively, and could be used as a new type of ratiometric fluorescence sensor for the detection of arginine.[52] Tan's group designed an acriflavine@-lanthanide metal–organic framework (Acr@Eu (BTEC)) by covalently combining an amino-rich dye (Acr) and a carboxyl-rich Eu (BTEC). The fabricated Acr@Eu (BTEC) exhibited two emission centers from Acr and Eu (BTEC). In the presence of ClO^-, the intense green fluorescence of Acr was significantly quenched while the unchanged red fluorescence emitted by

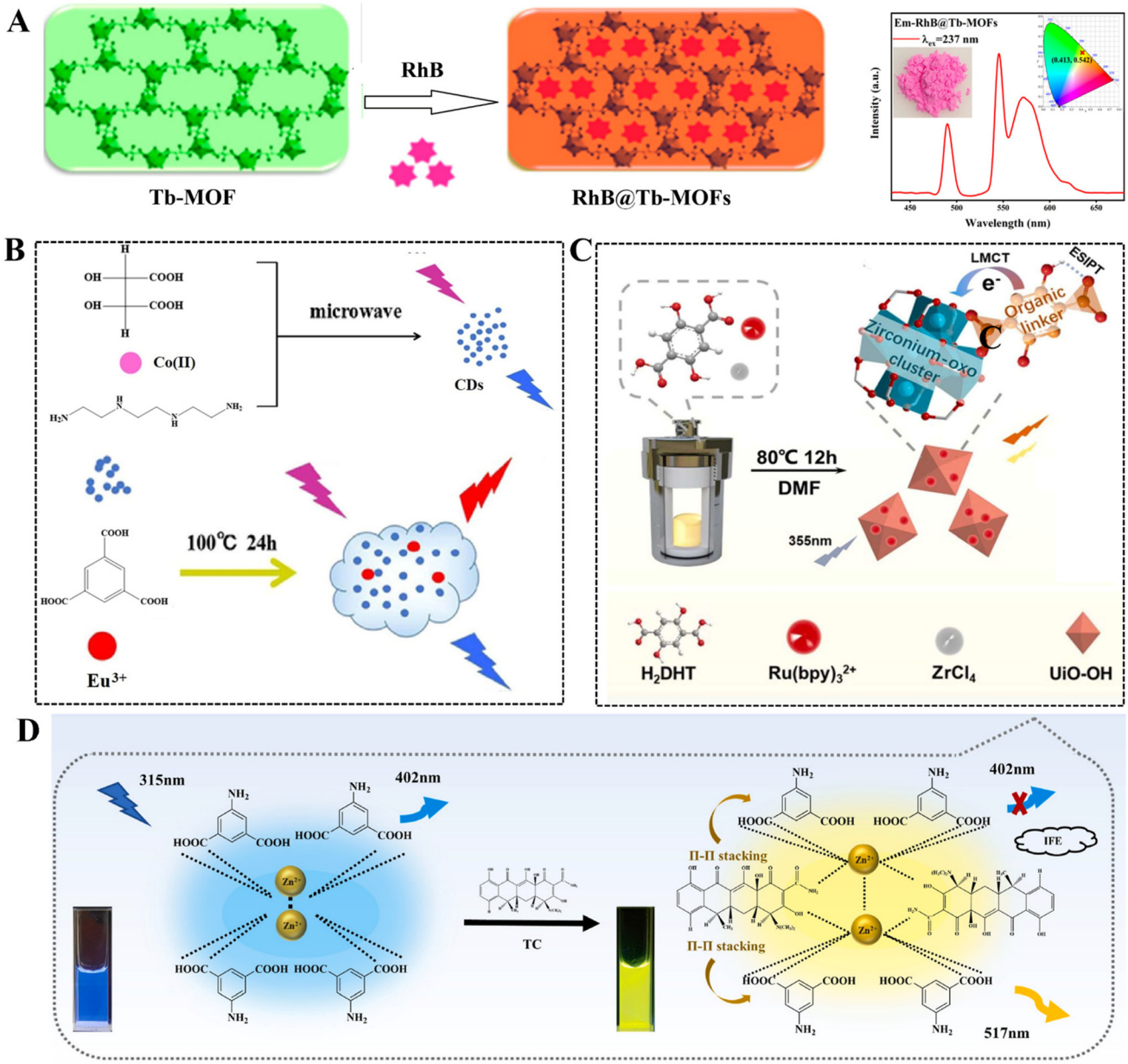

Fig. 5 Schematic preparation of dual-emission (A) RhB@Tb-MOFs,[51] (B) CDs@Eu-DPA MOFs,[55] and (C) Ru@UiO-OH.[67] (D) Schematic of TC-induced blue emission Zn-MOF-on-NH_2-MIL-53(Al) to produce a new emission.[69]

Eu^{3+} served as a reference signal. Therefore, Acr@Eu (BTEC) with two emission signals was developed as a ratiometric fluorescence sensor for the highly sensitive detection of ClO^-.[53]

5.2.2 Nanoparticles@MOFs. Since nanomaterials such as CDs, QDs, and metal nanoparticles exhibited the advantages of resistance to photobleaching, water dispersibility, and high fluorescence intensity,[54] the nanoparticles@MOF probes prepared by encapsulating luminescent nanomaterials in single-emission MOFs can not only exhibit the excellent properties of nanomaterials and single-emission MOFs, but also construct ratiometric fluorescence sensors for the enrichment and accurate detection of targets.

CDs are carbon particles less than 20 nm in size with excellent fluorescent properties. Wang *et al.* synthesized novel fluorescent CDs@Eu-2,6-pyridinedicarboxylic acid (DPA) metal–organic frameworks (MOFs) by encapsulating CDs in Eu-DPA MOFs (Fig. 5B). The CDs@Eu-DPA MOFs could emit two kinds of fluorescence from CDs and Eu-DPA MOFs under single wavelength excitation at 275 nm. In the presence of Cu^{2+}, the fluorescence of the Eu-DPA MOFs was quenched while that of the CDs remained unchanged, resulting in a ratiometric fluorescence response to Cu^{2+}.[55] Wei *et al.* encapsulated nitrogen/cobalt-doped carbon dots (N, Co-CDs) with strong blue light emission into red light-emitting europium metal–organic

frameworks (Eu-MOFs) by a self-assembly method. The prepared CDs@Eu-MOFs not only had good stability in aqueous solution but also exhibited dual-emission signals originated from CDs and Eu-MOFs. In the presence of chromium ions (Cr^{6+}), the fluorescence intensity of CDs decreased, while that of Eu-MOFs remained unchanged, so that a ratiometric fluorescence sensor could be constructed for the detection of Cr^{6+}.[56]

QDs are nanoscale semiconductors that emit light at a specific frequency under a certain electric field or light pressure.[57] Compared with ordinary organic fluorophores, QDs have obvious advantages such as high fluorescence yield, good photostability, and long fluorescence lifetime.[58,59] However, the high surface activity of QDs is subject to mutual agglomeration, which leads to fluorescence quenching. As a crystalline framework with porosity, large specific surface area and stability, MOFs can provide multiple binding sites for immobilized QDs and prevent their agglomeration. Here, Xu's group prepared a self-calibrated optical thermometer $CsPbBr_3$@Eu-MOF with a FQY greater than 50% by encapsulating $CsPbBr_3$ QDs into an Eu-MOF, which exhibited both green luminescence at 528 nm from $CsPbBr_3$ QDs and red luminescence at 618 nm from the Eu-MOF. As a result, the $CsPbBr_3$@Eu-MOF composite showed luminescence behavior with a dual-signal response to temperature and had the significant advantages of high sensitivity and high reliability.[60]

As common fluorescent metal nanoparticles, gold nanoclusters (AuNCs), silver nanoclusters (AgNCs) and copper nanoclusters (CuNCs) are promising for sensing and bioimaging due to their good optical properties,[61] low toxicity and small size.[62] To further improve the sensing performance of metal nanoparticles, MOFs have been chosen as carriers to improve their selectivity, sensitivity, and stability. For example, Shang's group prepared dual-emitting AuNCs@Eu-MOF from blue-fluorescent BSA-modified AuNCs and a red-fluorescent Eu-MOF for ratiometric fluorescence monitoring of adenosine triphosphate (ATP) by a one-step solvothermal method.[63] Similarly. Yan' group and Jing'group prepared dual-emission AgNCs (FQY = 8%)/metal–organic shell composite (FQY = 15%) and CuNCs@Tb@UiO-66-$(COOH)_2$ for phosphate and Cu^{2+} ratiometric fluorescence sensing, respectively.[64,65]

5.2.3 Luminescent complexes@MOFs. Cationic complexes of metals such as iridium and ruthenium have stable fluorescent properties in aqueous and organic solutions. To expand the applications of these complexes in photocatalysis, white light emission, biomedicine, and chemical sensing, they are encapsulated in metal–organic framework materials as luminescent guests. Zhang *et al.* encapsulated the iridium complex $[Ir(ppy)_2(bpy)]^+$ with yellow fluorescence in the pores of a blue-fluorescent MOF material. High-quality white light was observed by adjusting the concentration of the guest $[Ir(ppy)_2(bpy)]^+$, which effectively achieved a high QY (11.9%) and optimized white light emission.[66] Here, we focus on the encapsulation of luminescent complexes into MOFs for fluorescence sensing. Wang *et al.* encapsulated the red luminescent cationic complex $Ru(bpy)_3^{2+}$ into blue luminescent UiO-OH pores by a solvothermal method (Fig. 5C). At a single excitation wavelength, the fluorescence intensity of the prepared Ru@UiO-OH at 537 nm and 600 nm showed different variations as the concentration of the target trimethylamine (TM) increased. Since $Ru(bpy)_3^{2+}$ was stably encapsulated in the MOF pores, the constructed ratiometric fluorescence sensor exhibited high sensitivity, low detection limit, wide detection range, fast response, high stability, and reusability for TM.[67]

5.2.4 Target-induced new emission MOFs. In addition to the encapsulated approach described above, a particular strategy for constructing dual-emission MOFs is that the target induces a single-emission MOF to produce a new emission, which facilitates improved selectivity for the target. For example, Khalid M. proposed an ultra-small blue fluorescent zinc-based MOF (FMOF-5) and interestingly, tetracycline (TC) was able to adsorb onto the FMOF-5 surface and change the blue fluorescence of FMOF-5 (440 nm) to yellow-green fluorescence (520 nm) by aggregation-induced emission. As a result, the ratio $I_{520\ nm}/I_{440\ nm}$ of FMOF-5 allowed selective and accurate detection of TC.[68] In another research work, the target TC could cause quenching of the single characteristic peak of Zn-MOF-on-NH_2-MIL-53(Al) at 402 nm through an internal filtering effect, whereas the intrinsic green fluorescence of TC at 517 nm was enhanced through the coordination of the carboxyl group of TC to the metal active center Zn^{2+}. Thus, Zn-MOF-on-NH_2-MIL-53(Al) can be used as a reverse-ratio fluorescence sensor for TC detection (Fig. 5D).[69] Ding *et al.* prepared single-emission Tb-HDBB-CPNs (FQY = 14.27%), which exhibited a red fluorescence peak at 590 nm. With the addition of Zn^{2+}, Tb-HDBB-CPNs produced a new emission peak at 470 nm (FQY = 17.25%) due to ion exchange. Thus, a ratiometric fluorescence sensor was constructed based on the Tb-HDBB-CPNs for the detection of Zn^{2+}.[70]

5.3 Non-luminescent MOFs with other luminescent materials

In addition to luminescent MOFs, it has been reported that non-emissive MOFs can produce fluorescence by introducing mixed luminescent materials into their pores or binding luminescent materials to their surfaces. Thus, non-emissive MOFs can be used as a container for encapsulating mixed chromophores to form ratiometric fluorescence sensors. For example, Jia *et al.* used a one-step *in situ* synthesis method to simultaneously encapsulate blue fluorescent carbon dots (CDs) and red fluorescent InP/ZnS quantum dots (InPQDs) into ZIF-8. In the prepared CDs/InPQDs@ZIF-8, the InPQDs were used as the response units of the target and the CDs as reference signal units, which realized specific and sensitive ratiometric fluorescence sensing for Hg^{2+} and cysteine (Cys).[71] In addition, green luminescent fluorescein *o*-acrylate (F1) and red luminescent tris(2,2′-bipyridine)-diruthenium(II) hexahydrate (Rubpy) were simultaneously captured into the pores of the non-emitting Zn-MOF-74. The resulting F1/Rubpy@MOF showed dual-emission signaling. Interestingly, the addition of HClO could quench the green emission while the red emission was

unchanged, which made F1/Rubpy@MOF a ratiometric fluorescence sensor for HClO detection.[72]

6. Application

Based on the above dual-emission MOF construction strategy, we summarize the MOF-based ratiometric fluorescence sensors for pH, temperature, ions, biomarkers, and other applications over the last five years.

6.1 pH sensing

pH is an important parameter in biomedicine, food processing, analytical chemistry, new drug development, environmental monitoring, and so on. Research works on MOF-based ratiometric fluorescence sensors for pH detection are gradually being reported. As displayed in Fig. 6A, Yu *et al.* constructed a dual-emission 1-hydroxypyrene@Co/Tb-dipicolinic acid metal–organic framework (1-OHP@Co/Tb-DPA MOF) as a ratiometric fluorescence sensor for pH detection.[73] Under strong acids, the ligand DPA was protonated to form DPA-H$^+$, so its electronic structure was conducive to internal intramolecular charge transfer (ICT), thus weakening the antenna effect (energy transfer) from DAP to luminescent Tb^{3+}. The characteristic fluorescence peak of Tb^{3+} gradually increased with increasing pH, while the emission peak of the reference 1-OHP (396 nm) remained almost unchanged. This ratiometric fluorescence sensor exhibited an excellent linear response over the pH range of 0.3 to 5.0 and showed good visualization from blue to green. In addition, Ma *et al.* introduced the red luminescent center Eu-β-diketone into the blue luminescent multi-ligand UiO-66-NH_2 to construct dual-emission Eu(BTA)@CPP3 (Fig. 6B), which exhibited a wide range of sensing abilities in the pH range between 1.19 and 13.90 by protonation, inhibition of charge transfer and deprotonation.[74]

6.2 Ion sensing

Ion sensing plays an important role in the biomedical, chemical, and environmental fields.[75,76] For example, the arbitrary release of heavy metal Hg^{2+} poses a great threat to ecosystems and human health; hence, Shu *et al.* prepared a dual-emission $CsPbBr_3$@Eu-BTC nanocomposite (FQY = 57.33%) for the visual detection of Hg^{2+} by encapsulating $CsPbBr_3$ into Eu-BTC *via* an *in situ* growth method. As shown in Fig. 7A, in this sensing process, the red emission of the Eu-MOF remained unchanged while the green fluorescence of $CsPbBr_3$ was quenched, realizing an ultra-low detection limit of 0.116 nM for Hg^{2+} and a wide detection range of 0 to 1 μM.[77] Cu^{2+} is essential for the normal functioning and metabolism of human organs. Abnormal concentrations of Cu^{2+} can lead to the development of many diseases. Therefore, Xia *et al.* rationally designed dual-emitting Eu-DATA/BDC with a two-ligand strategy (Fig. 7B). Terephthalic acid (H_2BDC) was selected to sensitize Eu^{3+} for antenna-effect emission, while 2,5-diaminoterephthalic acid (H_2DATA) maintained its own luminescence for specific recognition of Cu^{2+}. This MOF-based ratiometric fluorescence sensor realized a fast response (less than 10 s), a wide detection range (1–40 μM) and a low detection limit (0.15 μM).[78] As a highly toxic and difficult-to-degrade metal ion, Pb^{2+} can enter the human body through food and drinking water, jeopardizing the function of the brain, kidneys, and nervous system.

In addition, as an important genetic and metabolic substance in living systems, phosphate ions are involved in many important physiological and pathological processes, and can be used as a direct marker for cardiovascular and acute kidney failure. Therefore, Yi *et al.* prepared a novel dual-response ratiometric fluorescent probe CDs/QDs@ZIF-8 by *in situ* encapsulation of blue-emitting CDs and red-emitting CdTe quantum dots (QDs) into zinc-metal–organic frameworks (ZIF-8) for ultra-highly selective and sensitive detection of Pb^{2+} and PO_4^{3-}

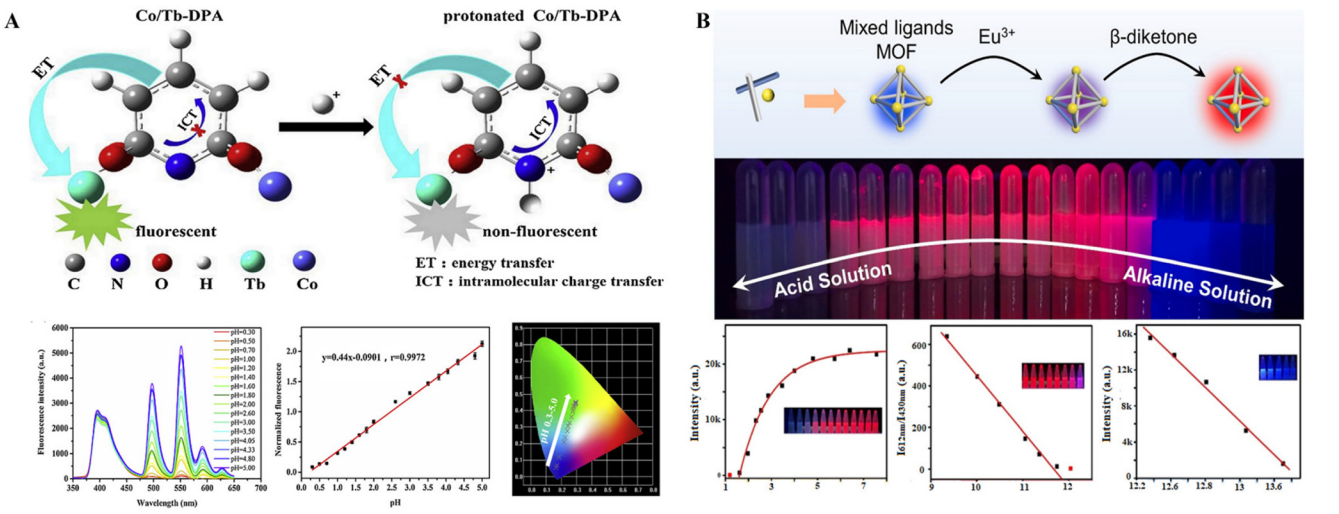

Fig. 6 pH sensing of MOF-based ratiometric fluorescent probes. (A) Schematic diagram of 1-OHP@Co/Tb-DPA MOF-based pH microsensor for visual detection of strong acids.[73] (B) Schematic diagram of dual-emission Eu(III)-functionalized multi-ligand MOFs for wide-range pH sensing.[74]

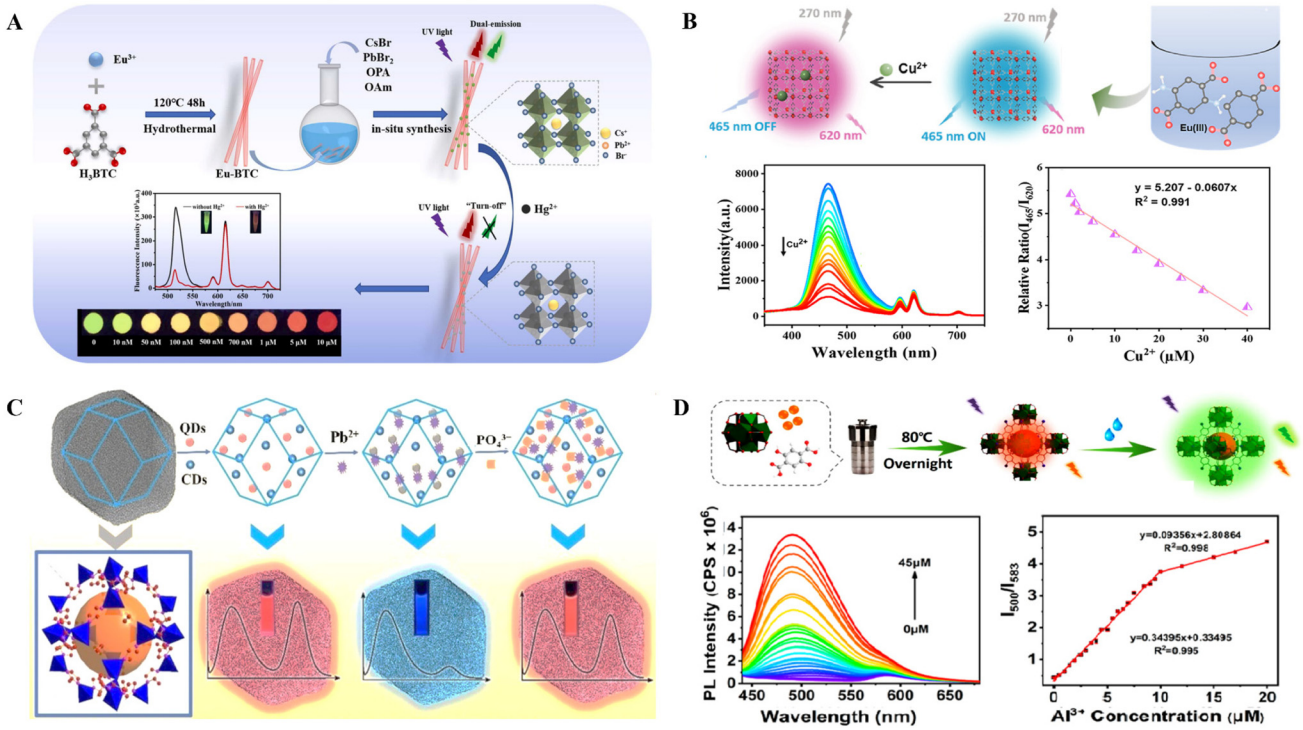

Fig. 7 Ion sensing of MOF-based ratiometric fluorescent probes. (A) Schematic diagram of the synthesis process of $CsPbBr_3$@Eu-BTC and the ratiometric fluorescence sensing of Hg^{2+}.[77] (B) Schematic diagram of ratiometric fluorescence sensing of Cu^{2+} in serum by Eu-DATA/BDC.[78] (C) Schematic diagram of CDs/QDs@ZIF-8 for ratiometric fluorescence sensing of Pb^{2+} and PO_4^{3-}.[79] (D) Schematic diagram of the preparation of UiO $(OH)_2$@RhB and the sensing process for Al^{3+}.[80]

(Fig. 7C). With the addition of Pb^{2+}, the CDs served as a stable internal standard, while mercaptoacetic acid on the surface of CdTe QDs combined with Pb^{2+} as well as the electrons of the photoexcited CdTe QDs transferred to the Pb^{2+}, thus quenching the fluorescence of the CdTe QDs. In contrast, the fluorescence of CdTe QDs was restored after the addition of PO_4^{3-} to the CDs/QDs@ZIF-8 + Pb^{2+} system. This ratiometric fluorescence signal responded linearly in the 0.04–60 μM and 0.25–50 μM ranges for Pb^{2+} and PO_4^{3-} with detection limits of 2.35 nM and 9.42 μM, respectively.[79] Excessive intake of Al^{3+} can promote the onset of Parkinson's disease, dementia, and Alzheimer's disease, so it is of great interest to construct a fast, effective, and simple method for the detection of Al^{3+}. Zheng *et al.* prepared dual-emission zirconium-based metal–organic framework composites ($UiO(OH)_2$@RhB) for ratiometric fluorescence sensing of Al^{3+} in aqueous media by a one-step solvothermal method (Fig. 7D). –OH on the surface of the green luminescent $UiO(OH)_2$was able to capture Al^{3+} in water through electrostatic and coordination affinity, which induced an excited state intramolecular proton transfer process and thus enhanced the fluorescence intensity, while the red fluorescence intensity of RhB remained stable. The sensor showed excellent sensitivity, good selectivity and fast response (2 min) to Al^{3+}, which was also applied to real food samples (grain legumes) with recoveries ranging from 89.08% to 113.61%.[80] Chen *et al.* prepared a novel effective dual-emission porphyrin metal–organic skeleton fluorescent probe by encapsulating $UiO\text{-}66(OH)_2$ into a porphyrin MOF (PCN-224), which showed excellent fluorescence performance in the detection of Cu^{2+}. In this probe, the signal of the encapsulated green-emitting $UiO\text{-}66(OH)_2$ was regarded as a reference signal, which could provide an effective in-built correction in complex environments. The red luminescent PCN-224 contained active sites for specific response to Cu^{2+}. As a result, the ratiometric fluorescence sensor provided a reliable platform for the detection of Cu^{2+} with LOD values as low as 0.068 nM. This LOD value is below the limit of Cu^{2+} concentration in drinking water.[81] Yu *et al.* synthesized a novel ratiometric fluorescent probe amino-functionalized S' Ln-MOF for the detection of F^- using Eu^{3+} as a metal node and 2′-amino-[1,1′:4′,1″-triphenylene]-3,3″,5,5″-tetracarboxylic acid ($H_4TPTC\text{-}NH_2$) as a ligand. The amino group not only adjusted the energy level of the benzene skeleton, but also provided a freely accessible site for F^-. Specifically, F^- could significantly increase the blue emission of the ligand and quench the red fluorescence of Eu^{3+} by hydrogen bonding with the amino group on the ligand backbone. As a result, dual-emission $EuTPTC\text{-}NH_2$ enabled efficient ratiometric fluorescence detection of F^- in aqueous solution with a fast response (60 s), a low detection limit (11.26 μM) and high selectivity.[82]

6.3 Temperature sensing

In 2012, Qian *et al.* prepared a temperature-responsive luminescent bimetallic Tb^{3+} and Eu^{3+} metal–organic framework,

which was firstly used as a temperature sensor with self-calibration function for cryogenic monitoring. Subsequently, the investigation of high-performance dual-signal MOF-based temperature sensors has been the focus of attention. As shown in Fig. 8A, Ding *et al.* constructed a dual guest-emitting zinc metal–organic framework (Cdots&RB@ZIF-8[2]) and embedded it into a flexible matrix for temperature sensing. Since the fluorescence resonance energy transfer that occurred between the two luminescent guests was heat dependent, the intensity ratio of C-dots to RBs exhibited excellent linear response to temperature in the physiological range of 20–80 °C with high sensitivity (0.74% $°C^{-1}$ at 20 °C), spectral reproducibility (>96%) and structural stability.[83] Gong *et al.* synthesized a blue-emitting NOb-type metal–organic framework (ZnNDPA) and formed a dual-emitting RhB@MOF fluorescent probe by adsorbing RhB (Fig. 8B). The fluorescence intensity ratio of the organic linker 5,5′-naphthalene-1,4-diyl-diisophthalic acid (H_4NDPA) to RhB showed a good linear relationship with temperature in the range of 30–90 °C, and the maximum relative temperature sensitivity was 0.42% $°C^{-1}$ at 30 °C.[84] Sun *et al.* synthesized a dual-emission fluorescent probe CdSe QDs/Eu-BTC by embedding green fluorescent CdSe QDs onto the surface of a red-emitting europium metal–organic framework (Eu-BTC) (Fig. 8C), which was further encapsulated into a hydrophobic film as a temperature-responsive material. Intriguingly, the material exhibited opposite photoluminescence behavior with increasing temperature. The fluorescence intensity ratio ($I_{618\ nm}/I_{530\ nm}$) of different luminescence centers showed high sensitivity (3.02% $°C^{-1}$) and a wide detection range (30 °C–110 °C) for temperature sensing.[85] Unlike the MOF-based luminescent composites constructed above, Li *et al.* prepared a single lanthanide MOF for temperature multimodal ratiometric fluorescence sensing by self-assembly of the ligand 2′,5′-dimethyl-[1,1′:4′,1″-terphenyl]-3,3″,5,5″-tetracarboxylic acid and Dy^{3+} ions. As shown in Fig. 8D, the thermally coupled energy level (TCEL)-based emis-

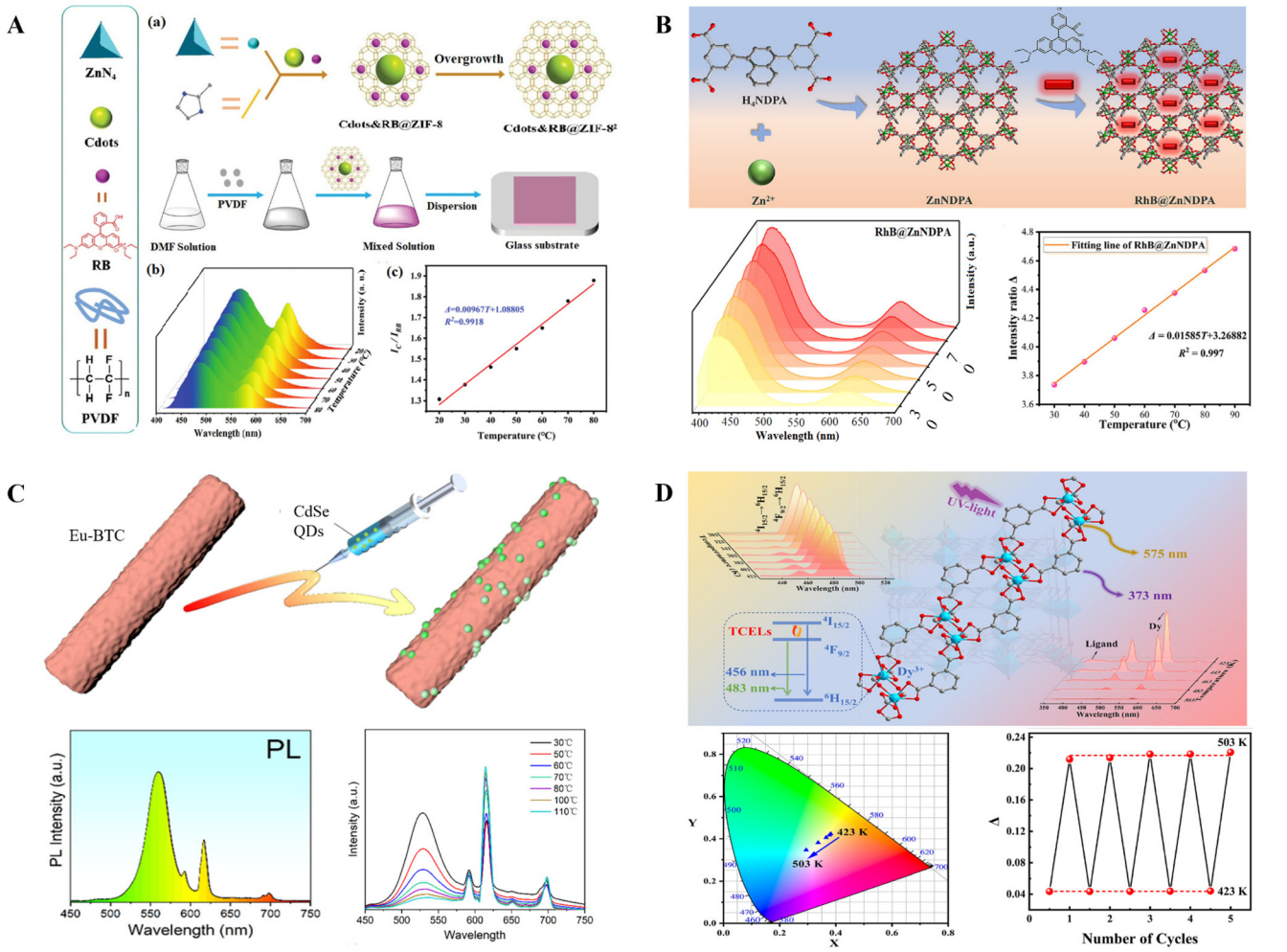

Fig. 8 Temperature sensing of MOF-based ratiometric fluorescent probes. (A) Schematic representation of synthesis of dual-emitting Cdots&RB@ZIF-8[2]-MMM and temperature sensing.[83] (B) Schematic of the preparation of RhB@MOF composites and temperature-ratiometric fluorescence sensing.[84] (C) Schematic diagram for the preparation of a CdSe/Eu-BTC composite material and the ratiometric fluorescence sensing of temperature.[85] (D) Schematic of Dy-MOF-based multimodal ratiometric fluorescence temperature sensing.[86]

sions of Dy^{3+} ($I_{456\ nm}/I_{483\ nm}$) have a distinct exponential relationship with temperature between 303 and 423 K, and the relative sensitivity at 30 °C was 1.20% K^{-1}. Another luminescence model parameter ($I_{343\ nm}/I_{575\ nm}$) of the ligand and Dy^{3+} displayed an S-type response to temperatures in the range of 423–503 K with a good sensitivity of 8.46% K^{-1} at 503 K.[86] Liu and team synthesized a series of mixed lanthanide metal–organic frameworks (M'LnMOFs) through a hydrothermal reaction, using 2-pyridyl-4-based 4,5-imidazole dicarboxylic acid (H_3PIDC) as the primary ligand and sodium oxalate as the auxiliary ligand. The MOFs could be utilized as ratiometric luminescent sensors for temperature detection, exhibiting a good linear response within the temperature range of 303 to 473 K.[87]

6.4 Biomarker sensing

Biomarkers are biochemical indicators that signify changes or potential changes in the structure or function of systems, organs, tissues, cells and subcells, and can be used in the diagnosis of disease. Many MOF-based ratiometric fluorescence sensors have been developed for the detection of biomarkers. As shown in Fig. 9A, Zhang's group reported a boronic acid covalent Eu-MOF (B-Eu-MOF) as a ratiometric fluorescence sensor for the detection of *N*-acetylneuraminic acid (NANA), a marker of lung cancer. The boronic acid structure on the surface of the B-Eu-MOF specifically bound to NANA and inhibited the antennae effect between the ligand and Eu^{3+}, which caused a decrease in the red spectrum and an increase in the blue spectrum. The fluorescence intensity ratio ($I_{470\ nm}/I_{614\ nm}$) of the B-Eu-MOF showed a detection limit of 1.23 mM for NANA in the detection range interval of 10^{-4} M–10^{-8} M.[88]

Su *et al.* successfully prepared ratiometric fluorescent probes CDs/QDs@MOFs for the detection of ascorbic acid (AA) and ascorbate oxidase (AAO) in serum by encapsulating blue-emitting carbon dots (CDs) and red-emitting thioglycolic acid (TGA)-capped CdTe QDs into Zn-MOFs (Fig. 9B). By switching the Hg^{2+} quenching signal on or off, the sensor could quantify AA and AAO in the ranges of 0.01–0.2 μM and 0.05–4 U L^{-1}, respectively.[89] Yang *et al.* synthesized a novel dual-emission hybrid fluorescent probe SiNPs/Tb-MOF for dipicolinic acid (DPA) detection by encapsulating blue-emitting SiNPs into a green-emitting Tb-MOF (Fig. 9C). In this sensing process, the addition of DPA enhanced the luminescence intensity of Tb^{3+},

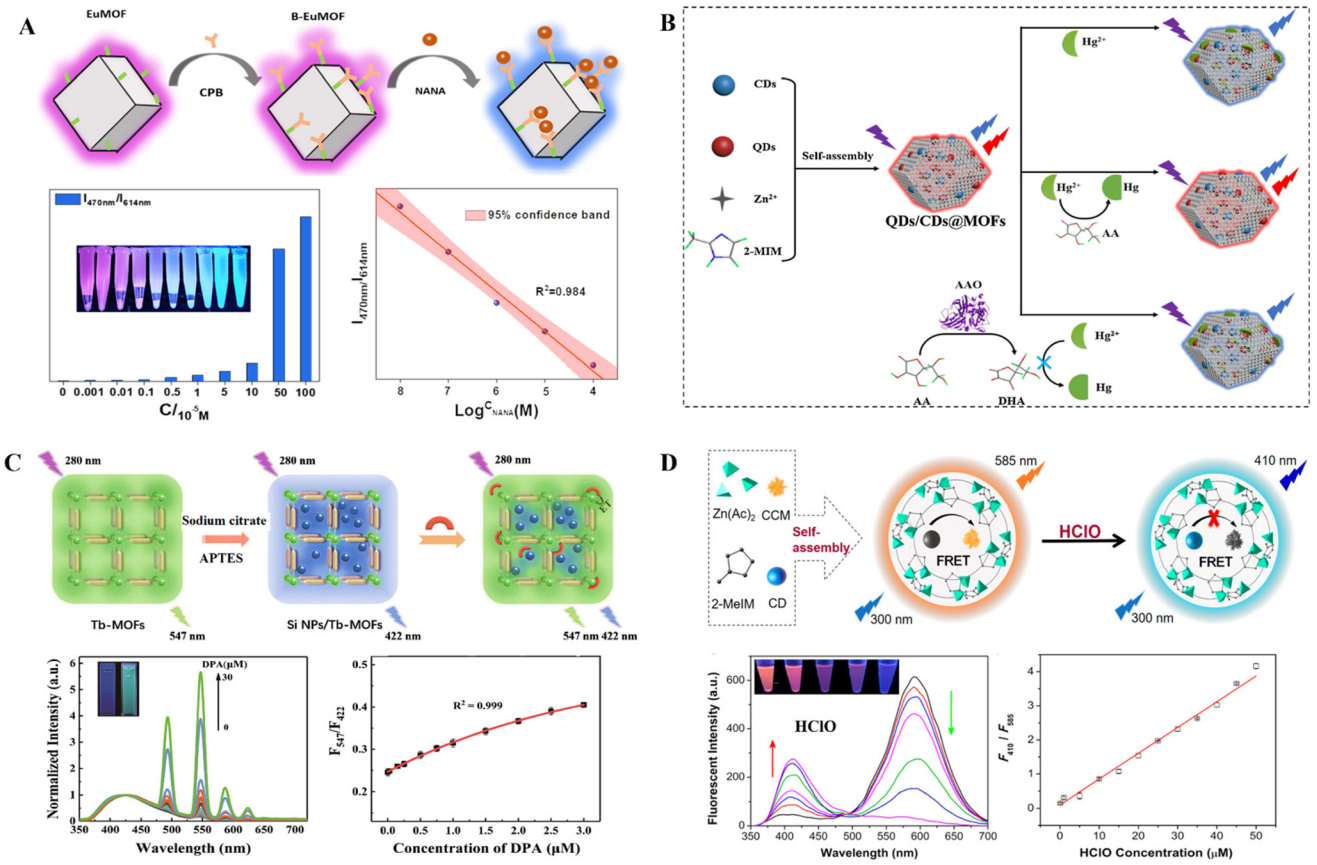

Fig. 9 Biomarker sensing of MOF-based ratiometric fluorescent probes. (A) Schematic representation of the dual emission B-Eu-MOF probe for NANA detection and the relationship of $I_{470\ nm}/I_{614\ nm}$ with different concentrations of NANA.[88] (B) Schematic representation of the synthesis of dual-emission QDs/CDs@MOFs and the ratiometric fluorescence sensing of AA and AAO.[89] (C) Schematic description of the preparation of Si NPs/Tb-MOFs and sensing process towards DPA.[90] (D) Schematic diagram of the synthesis of dual-emission CD/CCM@ZIF-8 and ratiometric fluorescence detection of HClO.[91]

while the fluorescence of SiNPs was unchanged. The sensor was able to provide a fast response (30 s) to DPA and achieved a low detection limit of 5.3 nM in the range of 0.025–3 μM.[90] As a biomarker for many diseases, the detection of hypochlorous acid is important for the assessment of physiological and pathogenetic processes. Therefore, Tan *et al.* encapsulated curcumin (CCM) and CDs into a Zn-MOF by a self-assembly method to construct a ratiometric fluorescence sensor for hypochlorous acid (HClO) detection (Fig. 9D). In the presence of HClO, *o*-methoxyphenol of CCM was oxidized to benzoquinone, thus inhibiting the fluorescence resonance energy transfer between CCM and CDs. As a result, the red fluorescence of CCM was enhanced while the blue fluorescence of CDs was quenched. Compared with other reactive oxygen species, the sensor achieved very high specificity for HClO and a low detection limit of 67 nM.[91] Unlike the above work, a new fluorescence sensor for detecting AA was developed by Zhang and colleagues by using luminol-incorporated iron-based metal–organic frameworks (luminol@Fe-DOBDC MOFs). The MOFs could emit fluorescence at two wavelengths, 430 nm and 540 nm, under excitation at 365 nm. Due to the ability of AA to reduce Fe^{3+} to Fe^{2+}, the fluorescence at 540 nm was significantly enhanced, while the fluorescence at 430 nm remained almost unchanged. As a result, the fluorescence ratio ($I_{540\ nm}$/$I_{430\ nm}$) of thedual-emission probe proved responsive to AA, showing a good linear relationship in the range of 0.2–30 μM, and the detection limit was as low as 70 nM.[92] Zhao and colleagues developed a sensor using terbium ions (Tb^{3+}) attached to the carboxyl groups of nanocage nickel metal–organic frameworks (NiMOFs). This Tb^{3+}@NiMOF sensor, created through post-synthesis modification involving coordination, featured Tb^{3+} ions as both secondary fluorescent sites and active sensing sites. It demonstrated high sensitivity, selectivity, and rapid response, along with excellent recyclability and a low detection limit (3.06 ng mL^{-1}). This sensor shows significant promise for direct and effective monitoring of serum epinephrine (EPI).[93] Yu *et al.* prepared dual-emission Tb-MOFs for the detection of alkaline phosphatase (ALP), and the obtained ratiometric fluorescent signal values were used to quantify ALP due to the fact that the phosphate ions, the enzymatic product between ALP and ascorbic acid phosphate sodium, could quench the emission of the Tb^{3+} ions and enhance the fluorescence of the ligand by blocking the ligand's energy transfer to Tb^{3+}.[94] Han *et al.* developed a DNA/MOF-based ratiometric fluorescence sensor to detect miRNAs by FRET. In this sensor, UiO-66-NH_2 MOFs were used as carriers to encapsulate RhB and capture DNA by forming Zr–O–P bonds; thiazolyl orange (TO) was preferentially intercalated into DNA to facilitate the encapsulation and thus formed double-emitting DNA-RhB@UiO-66-NH_2. The target miRNA could recover the fluorescence of TO by binding to the DNA-RhB@UiO-66-NH_2 probe *via* a strand displacement reaction.[95] Additionally, biomolecular recognition elements are often labeled on the interior or surface of dual-emission MOF structures through covalent bonding, adsorption, ligand exchange, and self-assembly methods to improve the recognition of target substances.[96–98]

6.5 Other sensing

In addition to the four prominent applications mentioned above, MOF-based ratiometric fluorescence sensors are also used in the sensing of drug residues, gases, humidity, and food spoilage. In drug residue sensing, organic disinfectants (quaternary ammonium salts and Cl/Br/I-containing compounds),[99] tetracycline,[100,101] cephalosporin,[102] pesticide residues of metribuzin,[103] *etc*. are common analytes. Due to the adsorption capacity of MOFs, Lu *et al.* prepared a blue-emitting zinc-based MOF with 2-(4-carboxyphenyl)-1*H*-benzo[*d*] imidazole-5-carboxylic acid (CBC) as the ligand for ratiometric fluorescence detection of oxytetracycline (OTC) (Fig. 10A). OTC was adsorbed onto the MOF surface and quenched the fluorescence of the Zn-MOF by an internal filtering effect (IFE), whereas the green fluorescence intensity of OTC was enhanced due to the aggregation-induced emission (AIE) of OTC in the Zn-MOF. (F^{540}/F_0^{540})/(F^{472}/F_0^{472}) showed a positive linear relationship with the amount of OTC with a detection limit of 26.9 nM.[104] Formaldehyde,[105] hydrogen sulfide (H_2S),[106] triethylamine,[107] *etc*. are common analytes in gas sensing. As shown in Fig. 10B, He *et al.* prepared novel vinyl-functionalized Eu-BDC-CH=CH_2 (Eu-MOF) for visual sensing of H_2S. The vinyl group of the ligand not only modulated the antenna effect of the ligand to Eu^{3+}, which led to an increase of purple fluorescence intensity at 363 nm and a decrease of red fluorescence intensity at 615 nm, but also served as the exposure reaction site of Eu-BDC-CH=CH_2 for the quantitative detection of H_2S. The designed ratiometric fluorescent probe showed the advantages of good acid–base stability (pH = 2–11), fast response (<2 min) and high sensitivity (LOD = 38.4 μM).[108]

Moisture sensing is essentially the detection of water and is generally used for quality control of solid drugs, chemicals, and food. Recently, MOF-based ratiometric fluorescence sensors have been applied to the determination of water content in honey,[111] the identification of water content in pharmaceuticals,[109] and the analysis of water content in organic reagents.[112] As shown in Fig. 10C, Xiao's group prepared a dual ligand dipicolinic acid/2-aminophthalic acid MOF (Eu-DPA/PTA-NH_2) for the determination of water content in pharmaceuticals. Since water could inhibit energy transfer from the first ligand DPA to Eu^{3+} as well as induce the intramolecular charge transfer of the second ligand aminophthalic acid (PTA-NH_2), the red fluorescence intensity of the Eu-DPA/PTA-NH_2 decreased while the blue fluorescence intensity was enhanced with the increase of water content. The B/R value showed a good linear relationship with the water content in the range of 0.5–5% v/v, and the LOQ was 0.30% (g/g) for water in granules and 0.14% (v/v) for water in capsules.[109] In addition, MOF-based ratiometric fluorescence sensors have been developed for the detection of biogenic amines and thus for the evaluation of food freshness.[15,67] By post-synthetic modification, Chen's group prepared the dual-

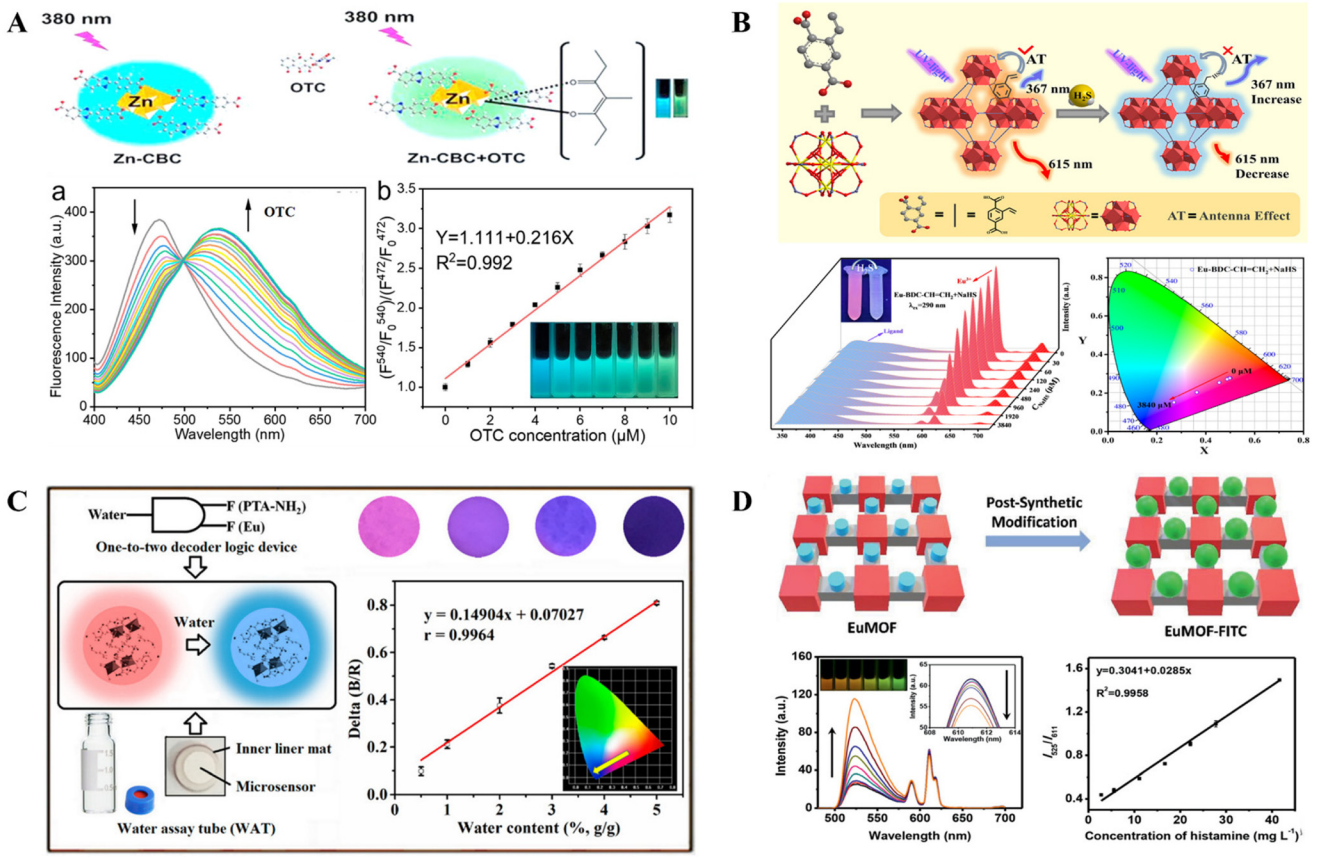

Fig. 10 Other sensing of MOF-based ratiometric fluorescent probes. (A) Schematic representation of OTC sensing with the fluorescent probe Zn-MOF.[104] (B) Schematic diagram of the synthesis of dual-emission Eu-BDC-CH=CH_2 and the ratiometric fluorescence sensing of H_2S.[108] (C) Schematic diagram of a dual-emission Eu-DPA/PTA-NH_2 based logic device for visual detection of water content in solid drugs.[109] (D) Preparation of dual-emission Eu-MOF-FITC and ratiometric fluorescence detection of BAs.[110]

emission fluorescent probe Eu-MOF-FITC by covalently coupling an amino-modified Eu-MOF and fluorescein 5-isothiocyanate (5-FITC) (Fig. 10D), which exhibited a reverse dual emission response to biogenic amines (BAs), with an enhancement of the emission of 5-FITC and a reduction of the emission of Eu^{3+}. The color of the sensor changed from red to green with the elevation of BAs and the fluorescence intensity ratio (I_{525}/I_{611}) was linearly proportional to BA concentration in the range of 2.78–41.67 mg L^{-1}, with the LOD value of 11 mg L^{-1}.[110] Above applications show that the dual-emission MOF-based ratiometric fluorescence sensors have obvious advantages in the analysis of complex sample matrices: (i) the self-calibration ability of the two emission peaks can reduce the influence of probe concentration and environmental changes on the detection results, enabling the sensors to maintain high accuracy and reliability in complex sample matrices; (ii) the dependence on the change of the ratio of dual-emission fluorescence intensity can enhance the sensitivity of the sensors to targets in complex matrices; (iii) the modification and surface functionalization of MOFs' structure can improve selectivity of the sensor in complex matrixes.

7. Conclusion and outlook

In conclusion, this review introduces the luminescence mechanism, typical synthesis methods, and sensing mechanism of dual emission MOFs and emphasizes the strategies for the construction of dual-emission MOF-based ratiometric fluorescence sensors, which are broadly categorized into three groups: intrinsic emission from mixed metals and ligands, encapsulation of luminescent guests into single-emission MOFs, introduction of mixed fluorophores into non-emission MOFs. These sensors have been successfully applied for pH, ion, temperature, biomarker, and other assays. Although dual-emission MOFs have made great strides in the field of fluorescence sensing, there are several issues that need to be addressed in the actual sample application. (i) The biocompatibility of dual-emission MOFs for *in vivo* sensing and *in situ* sensing attached to fresh food or body surfaces needs to be considered. Therefore, toxic metal ions, ligands, and luminescent guest molecules should be avoided when constructing MOF-based ratiometric fluorescence sensors. (ii) The stability of dual-emission MOF-based ratiometric fluorescence sensors in complex real sample environments needs to be further

improved. High stability allows the dual-emission MOFs to be recycled without affecting the sensing performance. The composition of dual-emission MOF-based composites is relatively complex and consideration of the structure and optical properties of additional emissive materials is required, which can easily lead to interface instability. Therefore, intrinsic dual-emission MOF-based ratiometric fluorescence sensors with their uniform structure and chemical homogeneity tend to be more stable. In addition, most dual-emission MOF ratiometric sensors do not maintain long-term stability in acidic and alkaline aqueous solutions, and the defects in the structure of the MOFs caused by the interaction between the sensors and the analyte can affect their repeatability as the detection cycle grows. Therefore, the selection of high-valent metal centers or multidentate ligands with high rigidity backbones as well as the introduction of stable luminescent guests and protectants offer the possibility of constructing stable MOF-based sensors. In addition, X-ray diffraction alone is not sufficient for evaluating the stability of dual-emission MOFs, which can only provide information on the post-sensing crystallinity. The residual porosity data of the MOF after sensing also need to be supplemented, which is crucial for the stability of the sensing performance. (iii) It remains a challenge to demonstrate MOF-based ratiometric fluorescence sensing mechanisms involving microscopic processes such as charge transfer solely based on experimental results. Therefore, a systematic study of the sensing mechanism through a combination of experimental and computational approaches is recommended to gain a comprehensive understanding of the fundamentals of the ratiometric fluorescence sensing process. (iv) Considering the specific response to the target, most MOF-based ratiometric sensors currently designed are highly sensitive and selective for the detection of a single analyte. Therefore, the development of high-throughput MOF-based ratiometric fluorescent array sensors is expected to achieve simultaneous accurate and highly sensitive detection of multiple targets in complex samples. (v) To overcome the disadvantages of fluorescence sensors that can only be operated in the laboratory, the development of portable smart analytical devices by integrating dual-emission MOF probes with flexible films and smartphones not only enables on-site analysis, but also will set a future trend in the development of smart sensors.

Considering the above challenges, we need to put more efforts to deepen our understanding on dual-emission MOF-based fluorescence sensors and to improve them in the future. We expect that dual-emission MOFs will have great potential as ratiometric fluorescence sensors in a wide range of analytical applications.

Author contributions

Shuxin Zhang: conceptualization, methodology, investigation, writing – original draft, writing – review and editing, and visualization. Jinyu Xiao: methodology, investigation, and writing – review and editing. Geng Zhong: conceptualization and investigation. Tailin Xu and Xueji Zhang: writing – review & editing, resources, project administration, and funding acquisition. All authors have read and agreed to the published version of the manuscript.

Conflicts of interest

There are no conflicts to declare.

Acknowledgements

We acknowledge funding from the Joint Fund of the Ministry of Education for Shenzhen University 2035 Program for Excellent Research (86901-00000221), the Equipment Pre-Research Project (8091B022142), the National Natural Science Foundation of China (22234006, 22104093), the Shenzhen Stability Support Plan (20200806163622001 and 20220809165141001), the Shenzhen Overseas Talent Program, and the Shenzhen Key Laboratory for Nano-Biosensing Technology (ZDSYS20210112161400001).

References

1 K. Wang, Y. Li, L.-H. Xie, X. Li and J.-R. Li, *Chem. Soc. Rev.*, 2022, **51**, 6417–6441.
2 M. Eddaoudi, J. Kim, N. Rosi, D. Vodak, J. Wachter, M. O'Keeffe and O. M. Yaghi, *Science*, 2002, **295**, 469–472.
3 W. Fan, X. Zhang, Z. Kang, X. Liu and D. Sun, *Coord. Chem. Rev.*, 2021, **443**, 213968.
4 H. Daglar, H. C. Gulbalkan, G. Avci, G. O. Aksu, O. F. Altundal, C. Altintas, I. Erucar and S. Keskin, *Angew. Chem., Int. Ed.*, 2021, **60**, 7828–7837.
5 A. N. Hong, H. Yang, X. Bu and P. Feng, *EnergyChem*, 2022, **4**, 100080.
6 A. Ahmad, S. Khan, S. Tariq, R. Luque and F. Verpoort, *Mater. Today*, 2022, **55**, 137–169.
7 A. C. Melvin, R. R. Tuttle, M. Mohnike and M. M. Reynolds, *ACS Mater. Lett.*, 2022, **4**, 2434–2439.
8 I. Ahmed, M. M. H. Mondol, M. J. Jung, G. H. Lee and S. H. Jhung, *Coord. Chem. Rev.*, 2023, **475**, 214912.
9 S. Zhang, L. Wang, T. Xu and X. Zhang, *ACS Appl. Mater. Interfaces*, 2023, **15**, 9110–9119.
10 G. Tian, Z. Zhou, M. Li, X. Li, T. Xu and X. Zhang, *Anal. Chem.*, 2023, **95**, 13250–13257.
11 Y. Chang, M. Chen, Z. Fu, R. Lu, Y. Gao, F. Chen, H. Li, N. Frans de Rooij, Y.-K. Lee, Y. Wang and G. Zhou, *J. Mater. Chem. A*, 2023, **11**, 6966–6977.
12 S. Mallakpour, E. Nikkhoo and C. M. Hussain, *Coord. Chem. Rev.*, 2022, **451**, 214262.
13 I. Abánades Lázaro and R. S. Forgan, *Coord. Chem. Rev.*, 2019, **380**, 230–259.
14 M. Ding, W. Liu and R. Gref, *Adv. Drug Delivery Rev.*, 2022, **190**, 114496.

15 S. Xing, S. Cheng and M. Tan, *Crit. Rev. Food Sci. Nutr.*, 2023, 1–17.
16 X. Wang, Y. Wang and Y. Ying, *TrAC, Trends Anal. Chem.*, 2021, **143**, 116395.
17 B.-B. Guo, J.-C. Yin, N. Li, Z.-X. Fu, X. Han, J. Xu and X.-H. Bu, *Adv. Opt. Mater.*, 2021, **9**, 2100283.
18 J. Liu, Z. Wang, P. Cheng, M. J. Zaworotko, Y. Chen and Z. Zhang, *Nat. Rev. Chem.*, 2022, **6**, 339–356.
19 K. T. Smith, K. Hunter, N.-C. Chiu, H. Zhuang, P. Jumrusprasert, W. F. Stickle, J. A. Reimer, T. J. Zuehlsdorff and K. C. Stylianou, *Angew. Chem., Int. Ed.*, 2023, **62**, e202302123.
20 L. Yang, Y. Song and L. Wang, *J. Mater. Chem. B*, 2020, **8**, 3292–3315.
21 Y.-R. Zhang, X.-Z. Xie, X.-B. Yin and Y. Xia, *Chem. Eng. J.*, 2022, **443**, 136532.
22 S. N. Nangare, A. G. Patil, S. M. Chandankar and P. O. Patil, *J. Nanostruct. Chem.*, 2023, **13**, 197–242.
23 P. Li, Z. Zhou, Y. S. Zhao and Y. Yan, *Chem. Commun.*, 2021, **57**, 13678–13691.
24 X. Luo, G. Huang, Y. Li, J. Guo, X. Chen, Y. Tan, W. Tang and Z. Li, *Appl. Surf. Sci.*, 2022, **602**, 154368.
25 Y. Ma, G. Xu, F. Wei, Y. Cen, X. Xu, M. Shi, X. Cheng, Y. Chai, M. Sohail and Q. Hu, *ACS Appl. Mater. Interfaces*, 2018, **10**, 20801–20805.
26 X. Fang, J. Ye, D. Duan, X. Cai, X. Guo and K. Li, *Microchim. Acta*, 2021, **188**, 204.
27 X. Qiao, Y. Han, D. Tian, Z. Yang, J. Li and S. Zhao, *Sens. Actuators, B*, 2019, **286**, 1–8.
28 S. Shakya and I. M. Khan, *J. Hazard. Mater.*, 2021, **403**, 123537.
29 A. P. de Silva, H. Q. N. Gunaratne, T. Gunnlaugsson, A. J. M. Huxley, C. P. McCoy, J. T. Rademacher and T. E. Rice, *Chem. Rev.*, 1997, **97**, 1515–1566.
30 J. Qiao, X. Chen, X. Xu, B. Fan, Y.-S. Guan, H. Yang and Q. Li, *J. Mater. Chem. B*, 2023, **11**, 8519–8527.
31 A. Sousaraei, C. Queirós, F. G. Moscoso, T. Lopes-Costa, J. M. Pedrosa, A. M. G. Silva, L. Cunha-Silva and J. Cabanillas-Gonzalez, *Anal. Chem.*, 2019, **91**, 15853–15859.
32 L. Chen, D. Liu, L. Zheng, S. Yi and H. He, *Anal. Bioanal. Chem.*, 2021, **413**, 4227–4236.
33 S. Xing, G. Zeng, X. Liu, F. Yang, Z. Hao, W. Gao, Y. Yang, X. Wang, G. Li, Z. Shi and S. Feng, *Dalton Trans.*, 2015, **44**, 9588–9595.
34 S. Xing, Q. Bing, L. Song, G. Li, J. Liu, Z. Shi, S. Feng and R. Xu, *Chem. – Eur. J.*, 2016, **22**, 16230–16235.
35 S. N. Zhao, L. J. Li, X. Z. Song, M. Zhu, Z. M. Hao, X. Meng, L. L. Wu, J. Feng, S. Y. Song, C. Wang and H. J. Zhang, *Adv. Funct. Mater.*, 2015, **25**, 1463–1469.
36 M. C. Heffern, L. M. Matosziuk and T. J. Meade, *Chem. Rev.*, 2014, **114**, 4496–4539.
37 M. Wu, Z. W. Jiang, P. Zhang, X. Gong and Y. Wang, *Sens. Actuators, B*, 2023, **383**, 133596.
38 D.-M. Chen, C.-X. Sun, Y. Peng, N.-N. Zhang, H.-H. Si, C.-S. Liu and M. Du, *Sens. Actuators, B*, 2018, **265**, 104–109.
39 Y. Zhang, B. Li, H. Ma, L. Zhang and Y. Zheng, *Biosens. Bioelectron.*, 2016, **85**, 287–293.
40 S. Yuan, L. Feng, K. Wang, J. Pang, M. Bosch, C. Lollar, Y. Sun, J. Qin, X. Yang, P. Zhang, Q. Wang, L. Zou, Y. Zhang, L. Zhang, Y. Fang, J. Li and H.-C. Zhou, *Adv. Mater.*, 2018, **30**, 1704303.
41 X.-B. Yin, Y.-Q. Sun, H. Yu, Y. Cheng and C. Wen, *Anal. Chem.*, 2022, **94**, 4938–4947.
42 J. E. Kwon and S. Y. Park, *Adv. Mater.*, 2011, **23**, 3615–3642.
43 W.-Q. Zhang, Q.-Y. Li, J.-Y. Cheng, K. Cheng, X. Yang, Y. Li, X. Zhao and X.-J. Wang, *ACS Appl. Mater. Interfaces*, 2017, **9**, 31352–31356.
44 X. Han, J. Liu, K. Yu, Y. Lu, W. Xiang, D. Zhao and Y. He, *Inorg. Chem.*, 2022, **61**, 5067–5075.
45 D. Wang, Q. Tan, J. Liu and Z. Liu, *Dalton Trans.*, 2016, **45**, 18450–18454.
46 L. Chen, D. Liu, J. Peng, Q. Du and H. He, *Coord. Chem. Rev.*, 2020, **404**, 213113.
47 C.-Y. Sun, X.-L. Wang, X. Zhang, C. Qin, P. Li, Z.-M. Su, D.-X. Zhu, G.-G. Shan, K.-Z. Shao, H. Wu and J. Li, *Nat. Commun.*, 2013, **4**, 2717.
48 M. Gutiérrez, Y. Zhang and J.-C. Tan, *Chem. Rev.*, 2022, **122**, 10438–10483.
49 H.-N. Wang, F.-H. Liu, X.-L. Wang, K.-Z. Shao and Z.-M. Su, *J. Mater. Chem. A*, 2013, **1**, 13060–13063.
50 M.-J. Dong, M. Zhao, S. Ou, C. Zou and C.-D. Wu, *Angew. Chem., Int. Ed.*, 2014, **126**, 1601–1605.
51 X. Jiang, W. Li, M. Liu, J. Yang, M. Liu, D. Gao, H. Li and Z. Ning, *Molecules*, 2023, **28**, 5847.
52 N. Song, Z. Zhai, L. Yang, D. Zhang and Z. Zhou, *J. Solid State Chem.*, 2023, **323**, 124025.
53 J. Xiong, Y. Xiao, J. Liang, J. Sun, L. Gao, Q. Zhou, D. Hong and K. Tan, *Spectrochim. Acta, Part A*, 2023, **285**, 121863.
54 Y. Shu, Q. Ye, T. Dai, Q. Xu and X. Hu, *ACS Sens.*, 2021, **6**, 641–658.
55 J. Hao, F. Liu, N. Liu, M. Zeng, Y. Song and L. Wang, *Sens. Actuators, B*, 2017, **245**, 641–647.
56 Y. Wang, J. He, M. Zheng, M. Qin and W. Wei, *Talanta*, 2019, **191**, 519–525.
57 M. Y. Gubin, A. V. Shesterikov, A. V. Prokhorov and V. S. Volkov, *Laser Photonics Rev.*, 2020, **14**, 2000237.
58 L. Jing, S. V. Kershaw, Y. Li, X. Huang, Y. Li, A. L. Rogach and M. Gao, *Chem. Rev.*, 2016, **116**, 10623–10730.
59 Z. Su, H. Shen, H. Wang, J. Wang, J. Li, G. U. Nienhaus, L. Shang and G. Wei, *Adv. Funct. Mater.*, 2015, **25**, 5472–5478.
60 J. Liu, Y. Zhao, X. Li, J. Wu, Y. Han, X. Zhang and Y. Xu, *Cryst. Growth Des.*, 2020, **20**, 454–459.
61 R. Jin, *Nanoscale*, 2015, **7**, 1549–1565.
62 Z. Luo, K. Zheng and J. Xie, *Chem. Commun.*, 2014, **50**, 5143–5155.
63 X. Zhou, X. Wang and L. Shang, *Chin. Chem. Lett.*, 2023, **34**, 108093.
64 P. Liu, R. Hao, W. Sun, Z. Lin and T. Jing, *Luminescence*, 2022, **37**, 1793–1799.

65 C. Dai, C.-X. Yang and X.-P. Yan, *Anal. Chem.*, 2015, **87**, 11455–11459.
66 S.-R. Zhang, G.-J. Xu, W. Xie, Y.-H. Xu and Z.-M. Su, *Inorg. Chem. Commun.*, 2021, **123**, 108359.
67 P. Jia, X. He, J. Yang, X. Sun, T. Bu, Y. Zhuang and L. Wang, *Sens. Actuators, B*, 2023, **374**, 132803.
68 S. S. Mohammed Ameen, N. M. Sher Mohammed and K. M. Omer, *Talanta*, 2023, **254**, 124178.
69 C. Wang, X. Luo, W. Lin, Y. Qi, W. Tang, J. Kong, J. Huang and Z. Li, *Dyes Pigm.*, 2023, **214**, 111229.
70 N. Lin, Q. Zhang, X. Xia, M. Liang, S. Zhang, L. Zheng, Q. Cao and Z. Ding, *RSC Adv.*, 2017, **7**, 21446–21451.
71 L. Zhang, Y. Xu, J. Xu, H. Zhang, T. Zhao and L. Jia, *J. Hazard. Mater.*, 2022, **430**, 128478.
72 K. Cai, M. Zeng, L. Wang, Y. Song and L. Chen, *ChemistrySelect*, 2019, **4**, 2649–2655.
73 L. Yu, Q. T. Zheng, D. Wu and Y. X. Xiao, *Sens. Actuators, B*, 2019, **294**, 199–205.
74 W. Ma, X. Quan and B. Yan, *Dyes Pigm.*, 2022, **206**, 110648.
75 R. R. Crichton, D. T. Dexter and R. J. Ward, *Coord. Chem. Rev.*, 2008, **252**, 1189–1199.
76 E. Gaggelli, H. Kozlowski, D. Valensin and G. Valensin, *Chem. Rev.*, 2006, **106**, 1995–2044.
77 Y. Shu, Q. Ye, T. Dai, J. Guan, Z. Ji, Q. Xu and X. Hu, *J. Hazard. Mater.*, 2022, **430**, 128360.
78 Y.-D. Xia, Y.-Q. Sun, Y. Cheng, Y. Xia and X.-B. Yin, *Anal. Chim. Acta*, 2022, **1204**, 339731.
79 K. Yi and L. Zhang, *J. Hazard. Mater.*, 2020, **389**, 122141.
80 X. Zheng, Y. Zhao, P. Jia, Q. Wang, Y. Liu, T. Bu, M. Zhang, F. Bai and L. Wang, *Inorg. Chem.*, 2020, **59**, 18205–18213.
81 J. Chen, H. Chen, T. Wang, J. Li, J. Wang and X. Lu, *Anal. Chem.*, 2019, **91**, 4331–4336.
82 K. Yu, Q. Wang, W. Xiang, Z. Li, Y. He and D. Zhao, *Inorg. Chem.*, 2022, **61**, 13627–13636.
83 Y. Ding, Y. Lu, K. Yu, S. Wang, D. Zhao and B. Chen, *Adv. Opt. Mater.*, 2021, **9**, 2100945.
84 M. Gong, Z. Li, Q. Wang, W. Xiang, T. Xia and D. Zhao, *J. Solid State Chem.*, 2022, **311**, 123147.
85 J. Sun, P. Zhang, K. Yan, A. Pan, F. Chen, J. Hong, C. Zhao, X. Chen and W. Xiong, *ACS Appl. Nano Mater.*, 2023, **6**, 12087–12094.
86 Z. Li, Q. Wang, K. Yu, W. Cui, Y. He, B. Chen and D. Zhao, *Inorg. Chem.*, 2023, **62**, 5652–5659.
87 Y. Yang, H. Huang, Y. Wang, F. Qiu, Y. Feng, X. Song, X. Tang, G. Zhang and W. Liu, *Dalton Trans.*, 2018, **47**, 13384–13390.
88 Y. Zhang, H. Lu and B. Yan, *Sens. Actuators, B*, 2021, **349**, 130736.
89 J. Chen, S. Jiang, M. Wang, X. Xie and X. Su, *Sens. Actuators, B*, 2021, **339**, 129910.
90 D. Yang, S. Mei, Z. Wen, X. Wei, Z. Cui, B. Yang, C. Wei, Y. Qiu, M. Li, H. Li, W. Zhang, F. Xie, L. Wang and R. Guo, *Microchim. Acta*, 2020, **187**, 666.
91 H. Tan, X. Wu, Y. Weng, Y. Lu and Z. Z. Huang, *Anal. Chem.*, 2020, **92**, 3447–3454.
92 K. Pei, J. Xu, D. Wu, L. Qi, L. Ma, R. Zhang and W. Qi, *Food Chem.*, 2024, **434**, 137417.
93 D. Zhao, W. Li, R. Wen, W. Li, X. Liu, X. Zhang and L. Fan, *J. Rare Earths*, 2023, DOI: **10.1016/jjre.2023.04.007**.
94 L. Yu, L. Feng, L. Xiong, S. Li, Q. Xu, X. Pan and Y. Xiao, *ACS Appl. Mater. Interfaces*, 2021, **13**, 11646–11656.
95 Q. Han, D. Zhang, R. Zhang, J. Tang, K. Xu, M. Shao, Y. Li, P. Du, R. Zhang, D. Yang, L. Zhang and X. Lu, *Sens. Actuators, B*, 2022, **361**, 131676.
96 N. Patel, P. Shukla, P. Lama, S. Das and T. K. Pal, *Cryst. Growth Des.*, 2022, **22**, 3518–3564.
97 Y. Zhao and D. Li, *J. Mater. Chem. C*, 2020, **8**, 12739–12754.
98 X. R. Wang, X. Z. Wang, J. Du, Z. Huang, Y. Y. Liu, J. Z. Huo, K. Liu and B. Ding, *J. Solid State Chem.*, 2019, **279**, 120949.
99 Q. Yang, F.-Y. Xie, J.-S. Wang, H.-Y. Yu, W.-T. Li, Y.-H. He, M. Pang, Y. Li and W.-J. Ruan, *Sens. Actuators, B*, 2022, **367**, 132041.
100 L. Jia, S. Guo, J. Xu, X. Chen, T. Zhu and T. Zhao, *Nanomaterials*, 2019, **9**, 976.
101 J. Zhang, Z. Bao, J. Qian, H. Zhou and K. Zhang, *Anal. Chim. Acta*, 2022, **1216**, 339991.
102 R. Jalili, M. H. Irani-nezhad, A. Khataee and S. W. Joo, *Spectrochim. Acta, Part A*, 2021, **262**, 120089.
103 Y. Yu, G. Huang, X. Luo, W. Lin, Y. Han, J. Huang and Z. Li, *Microchim. Acta*, 2022, **189**, 325.
104 Y. Lu, L. Yu, S. Zhang, P. Su, X. Li, X. Hao, S. Wang and M. Sun, *Appl. Surf. Sci.*, 2023, **625**, 157202.
105 C. M. Li, J. P. Huang, H. L. Zhu, L. L. Liu, Y. M. Feng, G. Hu and X. B. Yu, *Sens. Actuators, B*, 2017, **253**, 275–282.
106 K. Yu, Q. Wang, Z. Li, Z. Xin, X. Han, T. Alshahrani, Y. He, D. Zhao and B. Chen, *Microporous Mesoporous Mater.*, 2023, **356**, 112594.
107 X.-C. Yang, S.-Q. Fu, Q.-L. Li, Z. Jiao, J.-T. Zhao, Y. Guo, Z.-J. Zhang, S. Gao and L.-L. Cheng, *Chem. Eng. J.*, 2023, **465**, 142869.
108 X. Han, J. W. Liu, K. L. Yu, Y. T. Lu, W. Q. Xiang, D. Zhao and Y. B. He, *Inorg. Chem.*, 2022, **61**, 5067–5075.
109 L. Yu, Q. T. Zheng, H. Wang, C. X. Liu, X. Q. Huang and Y. X. Xiao, *Anal. Chem.*, 2020, **92**, 1402–1408.
110 J. Wang, D. Li, Y. Ye, Y. Qiu, J. Liu, L. Huang, B. Liang and B. Chen, *Adv. Mater.*, 2021, **33**, e2008020.
111 C. Guan, J. Cai, X. Liu and L. Guo, *Sens. Actuators, B*, 2022, **355**, 131323.
112 H. Q. Yin, J. C. Yang and X. B. Yin, *Anal. Chem.*, 2017, **89**, 13434–13440.